Clays and Clay Minerals, Vol. 68, No. 3:189–196, 2020

MODIFICATION OF HALLOYSITE NANOTUBES FOR ENHANCEMENT OF GAS-ADSORPTION CAPACITY

Sungho Lim, Sooji Park, and Daewon Sohn*

[1]Department of Chemistry and Research Institute for Convergence of Basic Science, Hanyang University, Seoul 04763, Korea

Abstract—Structure control and quantitative evaluation of porous materials are essential for many industrial and consumer applications of clay minerals, and nanotubular halloysite (HNT) has been used extensively for such purposes; performance enhancements are still needed, however. The objective of the present study was to improve the gas-adsorption capacity of HNT by controlling the particle size and porosity. This was accomplished through acid treatment and particle-size fractionation by centrifugation. Various particle sizes were obtained and porosities ranged from macropores to mesopores. Natural halloysite nanotubes were modified by sulfuric acid in various concentrations to selectively remove the alumina composition of the tubes. X-ray diffraction and energy dispersive X-ray spectroscopy were used to verify the mineralogical and compositional changes. Surface modification by the acid treatment increased the inner space volume of the tubes and decreased the mass of the nanotubes because of the elimination of alumina. The gas adsorption capacity of both natural and modified halloysite nanotubes was measured quantitatively using N_2 adsorption and the Brunauer-Emmett-Teller (BET) method, and the morphology was determined from transmission electron microscopy (TEM) images. The results showed that the modified halloysite nanotube was 7.47 times more efficient at gas adsorption than pristine halloysite. Moreover, the dealumination of the surface increased the inner space. Greatly increased porosity characteristics, including gas adsorption and macroporosity, were obtained through modification by acid treatment.

Key Words—Gas adsorption · Halloysite · Porous materials · Selective surface modification

INTRODUCTION

Halloysite is a natural aluminosilicate nanotube with the formula $Al_2Si_2O_5(OH)_4$, a kaolin mineral. This clay material has tube walls that are 20–30 layers thick, with each layer consisting of one alumina (Al-OH) sheet and one siloxane (Si-O-Si) sheet (a one-to-one ratio), thus forming multiple inorganic walls. The inner wall surface is composed of alumina units, and the outer surface area is made of siloxane units. The diameter of the lumen (hollow space or channel inside the tube) ranges from 20 to 30 nm and the outer diameter from 50 to 100 nm (Tazaki 2005; Kamble et al. 2012; Joo et al. 2013; Lvov et al. 2016).

Halloysite nanotubes (HNTs) are of great interest due to their porosity as tubular structures, having specific mesoporosity (<50 nm) and macroporosity (>50 nm) characteristics (Shu et al. 2015). These nano spaces have great potential for use in the creation of nanocomposites in clay materials.

HNTs are utilized frequently as additives to other materials (Mroczek et al. 2011; Hong et al. 2013). Owing to their tubular shape with a hollow inside, they can be used as carriers (Shi et al. 2011; Tan et al. 2013; Owoseni et al. 2014; Gorrasi 2015) or nanoreactors (Ko et al. 2016). The confinement of nanomaterials in nanotube formations generates nanoscale reactions (Abdullayev et al. 2011; Lazzara et al. 2018). Various studies on surface modification aimed at utilizing the lumen have been reported (Yah et al. 2012a, 2012b; Chao et al. 2013; De Silva et al. 2013; Wu et al. 2013, 2016; Szczepanik et al. 2017). HNT nanocomposites are useful for remedying the shortcomings of base materials. The eco-friendly and biocompatible properties of HNTs are likewise important characteristics (Vergaro et al. 2010; Liu et al. 2012; Lvov et al. 2014; Massaro et al. 2014). These properties, which provide great advantages in applied research, originate from the aluminosilicate composition, which is not harmful to organisms or to the natural environment. Various studies have utilized this biocompatibility for drug-delivery systems and the controlled release of medicines (Guo et al. 2012; Xi et al. 2013).

Because the lumen is the main reason for the interest in using HNTs in applied research, detailed analysis of these nano spaces is necessary. Although natural, meaning unmodified, HNTs have adequate inner space volume to put various chemicals in the tube, the gas adsorption capacity and the surface area can be increased significantly by modifying the HNTs. The alumina composition of HNTs can be removed by sulfuric acid, because sulfuric acid selectively reacts with only the alumina sheets (Abdullayev et al. 2012; Zhang et al. 2012).

The purpose of the present study was to chemically modify the HNTs by treatment with sulfuric acid in an effort to enhance the storage efficiency of the tubes and to quantify the gas-adsorption capacity, then to compare the lumen surface area of the sulfuric-acid-modified HNTs with that of unmodified HNTs.

EXPERIMENTAL

Materials

HNTs were obtained from Applied Minerals Inc. (New York, USA). Sodium hexametaphosphate (Junsei Co., Tokyo, Japan, 97% purity) and sulfuric acid (Daejung Co., Seoul, Korea, 98% purity) were used without further purification.

* E-mail address of corresponding author: dsohn@hanyang.ac.kr
DOI: 10.1007/s42860-019-00059-4

Modification of Natural HNTs

A 1.5 g portion of HNT was mixed with 50 mL of 1 M, 3 M, or 5 M sulfuric acid solution in a flask. The HNT was well dispersed in the acid solution by bath-type sonication for 20 min. An aspirator was used to remove atmospheric gases from the lumen of the tubes. As a result, the sulfuric acid solution from the flask filled the lumen of the halloysite nanotubes, and chemical reactions occurred to remove the alumina composition of the HNT. The flask was heated at 90°C for 24 h to react the sulfuric acid with the aluminum of the HNT (Abdullayev et al. 2012). After reaction, the HNT modified by the 1 M, 3 M, and 5 M sulfuric acid were labeled "yHNT (*x* M)", where y is the modification and *x* is 1, 3, or 5, depending on which sulfuric acid concentration was used. The sample was then washed with DI water 5 times, placed in a freezer for 6 h, and freeze dried for 3 days.

Purification and Separation of Natural HNTs

Purification of the unmodified HNTs followed the method introduced by Luo et al. (2013). 25 g of HNT was suspended in 100 mL of DI water by stirring for 2 h; then 2 g of sodium hexametaphosphate (SHMP) was added gradually to enhance dispersion. The system was then stirred for an additional 24 h and left to stand at room temperature for 6 h to allow solids to settle. The supernatant was decanted and discarded to remove readily soluble impurities. The remaining solid was then separated into various size fractions by centrifugation as follows. The sediment was resuspended in water then centrifuged at 2000 rpm (431×*g*) for 5 min and the supernatant collected and labeled HNT-1. The sediment was again resuspended in water and centrifuged at 4000 rpm (1722×*g*) for 10 min and the supernatant decanted and labeled HNT-2. These steps were repeated at 6000 rpm (3875×*g*), 8000 rpm (6888×*g*), and 10,000 rpm (10,763×*g*) to obtain samples labeled HNT-3, HNT-4, and HNT-5, respectively. This was repeated for each HNT specimen. Each such particle-size fractionation yielded tubes with different average lengths and outer and inner diameters (Table 4).

Acid Modification of HNT

A 0.5 g portion of each mHNT-*x* (m = modification; *x* = 1–5) sample was mixed with 16.7 mL of 5 M sulfuric acid in a flask and further dispersed by vortex mixing and sonication. The suspension was then aspirated to remove dissolved gases in the HNT suspension in order to facilitate the entrance of sulfuric acid solution into the lumen, thereby enabling reaction between the sulfuric acid and the Al in the tetrahedral sheet of the HNT inner wall. The reaction was further promoted by heating the suspensions at 90°C for 24 h. They were then cooled, washed five times with DI water, and freeze-dried. The process was repeated for all HNTs.

RESULTS AND DISCUSSION

Modification of Natural HNTs

The porosities and surface areas of the HNTs were measured using N_2 adsorption. The volume of adsorbed gas at standard state (STP: $T = 273.15$ K, 101.3 kPa) per g of sample, represented by V_a, was measured by the Brunauer-Emmett-Teller (BET) method using a Belsorp-Mini II device (MicrotracBEL Corp., Osaka, Japan). Adsorption of volumetric N_2 proceeded on unmodified and modified HNTs. The N_2 gas-adsorption capacity of the unmodified HNT was 163.74 cm^3 (STP)/g. The isotherm type was IUPAC type IV, revealing pore sizes in the mesoporous and macroporous ranges, but not in the microporous range. In the case of mHNTs (1 M), the value of V_a was 471.14 cm^3 (STP)/g; for mHNTs (3 M), 746.75 cm^3 (STP)/g. The value of V_a for mHNTs (5 M) was 837.31 cm^3 (STP)/g, which is 5.11 times greater than for the natural HNTs (Table 1). All modified HNTs exhibited morphologies and plot shapes that follow the IUPAC type IV isotherms, similar to the natural HNTs.

The thickness of the adsorption layer is defined as $t = 0.354 \times V_a/V_m$ [nm]. The value of 0.354 comes from the assumption that the thickness of a single layer of N_2 molecules is 0.354 nm (Lippens and De Boer 1965; Kaneko 1994). According to one hypothesis, adsorbed N_2 molecules form an hexagonally close-packed layer on the solid surface (Schull 1948). The linear-like graph shapes of the samples in Fig. 1b, which increase at the same rate as standard isotherms, means that they have macroporous characteristics. The graphs of the modified HNTs have a steeper slope than those for unmodified HNTs. This is because the V_m values, which indicate the monolayer volume of the samples, are larger in the modified HNTs. The V_a value of mHNTs (5 M) at 1.2 nm of pore thickness was 270.17 cm^3 (STP)/g, which is 8.5 times larger than the V_a value of the natural HNTs of 31.703 cm^3 (STP)/g at 1.2 nm. The modified HNTs had a larger capacity for gas-adsorption than the natural HNTs.

The internal structures of the natural HNTs and the mHNTs were revealed by transmission electron microscopy (TEM, JEOL JEM-2100F, Tokyo, Japan) (Fig. 2). A clear crystal morphology with a relatively small lumen diameter in the natural HNTs was verified. In contrast, the mHNTs lost their crystallinity after dealumination, and their lumen diameter was expanded.

The crystallinities of both natural HNTs and modified HNTs were analyzed using X-ray diffraction (XRD). The diffraction patterns of natural HNTs have a monoclinic-domatic crystallographic character. The characteristic sharp peak at 12°2θ (Fig. 3) corresponding to the (001) reflection occurred due to the HNT multiwall reflection (Costanzo and Glese 1985; Guimaraes et al. 2010). Modified HNTs lost the characteristic peaks in the corresponding 2θ region, however.

Table 1 Adsorbed gas volume (V_a), specific surface area (S_{BET}), and total pore volume (V_{total}) of natural HNT, mHNT (1 M), mHNT (3 M), and mHNT (5 M).

	V_a (cm^3(STP)g^{-1})	S_{BET} (m^2g^{-1})	V_{total} (cm^3g^{-1})
HNT	163.74	34.076	0.2533
mHNT (1 M)	471.14	185.41	0.7288
mHNT (3 M)	746.75	232.26	1.1551
mHNT (5 M)	837.31	280.64	1.2951

https://doi.org/10.1007/s42860-019-00059-4 Published online by Cambridge University Press

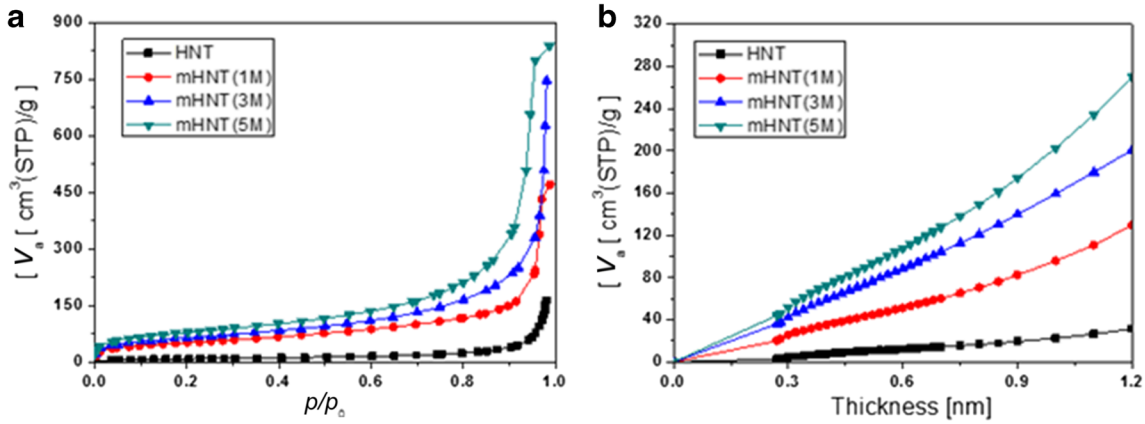

Fig. 1 **a** N_2 adsorption isotherms and **b** thickness plots of natural HNT, mHNT (1 M), mHNT (3 M), and mHNT (5 M).

Instead of the sharp peaks indicating alumina crystals, modified HNTs showed a broad band observed at ~20–25°2θ. This means that the aluminosilicate composition of the natural HNTs was changed to amorphous silica by acid modification.

Energy-dispersive X-ray spectroscopy (EDS) mapping was used to track changes in elemental composition and to verify structural changes during acid modification. Comparison of unmodified and modified HNTs (Fig. 4) revealed that the unmodified HNT was composed of evenly combined and distributed Al, Si, and O, whereas EDS mapping of the mHNTs (5 M) sample revealed that most of the Al was lost but the morphology of the silica structure remained.

Modification of Separated HNTs

The five particle-size fractions of the unmodified HNT (using the BET method) yielded similar shapes in their gas-

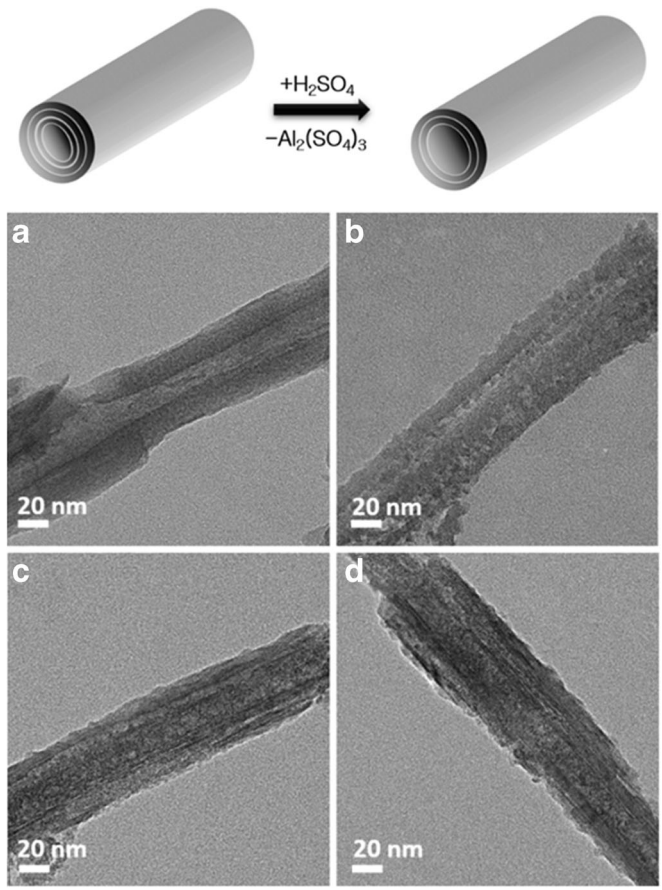

Fig. 2 TEM images of: **a** natural HNT, **b** mHNT (1 M), **c** mHNT (3 M), **d** mHNT (5 M).

https://doi.org/10.1007/s42860-019-00059-4 Published online by Cambridge University Press

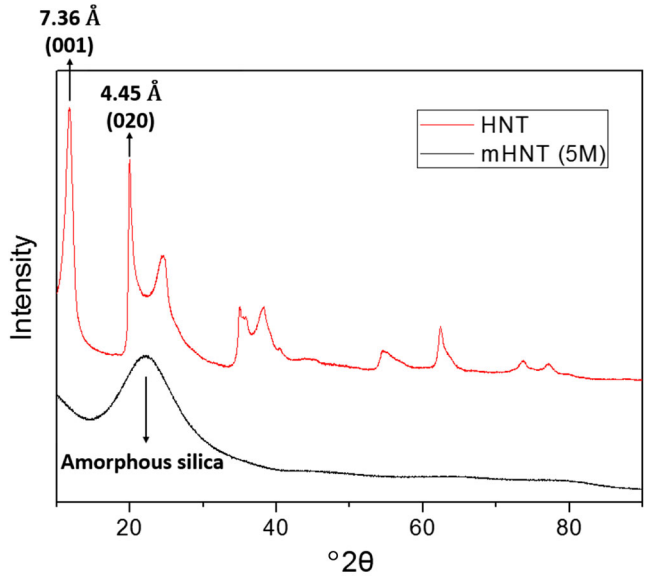

Fig. 3 XRD traces of natural HNT and mHNT (5 M).

adsorption isotherms (type IV), as would be expected because of their similar atomic compositions and morphologies. A notable difference, however, was in the value of V_a, which is a reflection of characteristics such as size, mass, and porosity. The samples showed a consistent tendency of increasing V_a, except for HNT-5, which was assumed to differ because of an imperfect structure in the tubes that hindered gas adsorption.

The largest value for V_a was 226.43 cm^3 (STP)/g, for HNT-4. This was 1.74 times larger than the smallest V_a value, which was exhibited by HNT-1 (130.37 cm^3 (STP)/g. Another trend was that the adsorption capacity increased consistently in the lower p/p_0 range, from HNT-1 to HNT-5 (Table 2).

Compared to those of unmodified HNTs (Fig. 5a), the adsorption isotherms of the five particle-size fractions of the acid-modified HNTs revealed a consistent tendency for the V_a value to decrease as the particle size became smaller (Fig. 5b). The largest V_a was 1223.1 cm^3 (STP)/g, for mHNT-5, which was 5.6 times larger than for HNT-5 before acid treatment (Tables 2 and 3). The results showed that the modification of halloysite nanotubes increased the gas-adsorption efficiency of the unmodified halloysite by a factor of 7.47 (1223.1/163.74) (Tables 1 and 3). Overall, acid modification of the HNT increased its porosity, gas-adsorption capacity, and macroporosity. The smallest value for V_a among the mHNT samples was 638.84 cm^3 (STP)/g for mHNT-1, which is 4.9 times larger than for HNT-1. Both acid activation and smaller particle size improved the gas-adsorption capacity of HNT tubular materials, therefore.

The porosity distributions of the HNTs were plotted using the Barrett-Joyner-Halenda (BJH) method. Adsorbents that have type IV adsorption isotherms can be characterized by BJH adsorption-desorption plots (Luan et al. 1995; Baiju et al. 2009). Hysteresis, the difference between adsorption and desorption curves, occurs due to capillary condensation of N_2 gas in the mesopores of the materials (Barrett et al. 1951). The desorption isotherm of the material and the Kelvin

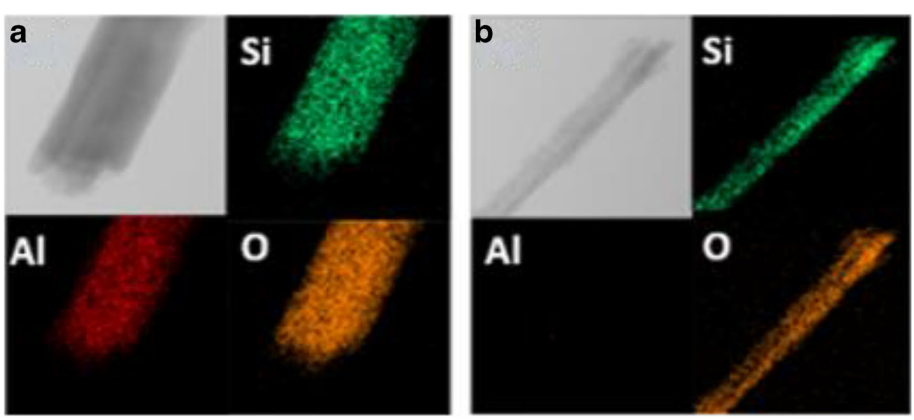

Fig. 4 EDS mapping images of **a** natural HNT and **b** mHNT (5 M).

https://doi.org/10.1007/s42860-019-00059-4 Published online by Cambridge University Press

Table 2 Adsorbed-gas volume (V_a), specific surface area (S_{BET}), and total pore volume (V_{total}) of 5 groups of natural HNTs.

	V_a (cm^3(STP)g^{-1})	S_{BET} (m^2g^{-1})	V_{total} (cm^3g^{-1})
HNT-1	130.37	26.866	0.2017
HNT-2	191.74	29.515	0.2966
HNT-3	209.32	31.042	0.3238
HNT-4	226.43	67.378	0.3502
HNT-5	217.93	73.373	0.3371

Table 3 Adsorbed gas volume (V_a), specific surface area (S_{BET}), and total pore volume (V_{total}) of five groups of mHNTs (5 M).

	V_a (cm^3(STP)g^{-1})	S_{BET} (m^2g^{-1})	V_{total} (cm^3g^{-1})
mHNT-1	638.84	124.61	0.9820
mHNT-2	689.00	134.73	1.0657
mHNT-3	866.50	166.64	1.2656
mHNT-4	906.43	185.07	1.4020
mHNT-5	1223.1	202.24	1.8919

equation (Eq. 1) demonstrate the relationships between critical condensation pressure and pore size and were used to calculate the pore-size distribution in the BJH plots (Schull 1948).

$$\ln\frac{p}{p_0} = -\frac{2\gamma V_L}{RTr_m} \quad (1)$$

where p is equilibrium pressure in pores with a radius r_m; p_0, pressure on the planar surface; γ, the surface tension; V_L, the molar volume; R, the gas constant; and T, the absolute temperature. The cumulative pore-volume graph was obtained for various pore volumes. The observed tendency (Fig. 6a) was that the pore size decreased from HNT-1 to HNT-5. Samples HNT-1 and HNT-2 were macroporous, whereas HNT-3, HNT-4, and HNT-5 were mesoporous. HNT-1 exhibited the tallest peak at d_p = 70 nm, revealing obvious microporous behavior. On the other hand, sample HNT-5 was mesoporous because the porosity distribution was clearly <50 nm. Because the volume distributions of HNT-4 and HNT-5 were close to 0 with a porosity distribution >50 nm, these samples were non-macroporous tubes.

Plots of the BJH curves for the five groups of modified HNTs (Fig. 6b) revealed that the porosities of all natural HNTs were expanded by sulfuric acid modification. The pore sizes of samples mHNT-3, mHNT-4, and mHNT-5 (on the right side of Fig. 6b) compared to those of the natural HNTs groups were enlarged from mesopores to macropores.

Regarding pore-thickness curves of the separated HNTs7, the slopes of the curves increased with decreasing particle size (Fig. 7a). This indicates that samples separated later had larger V_m values and gas-adsorption efficiencies. The gas adsorption of mHNT-5 at 1.2 nm pore thickness was 83.816 cm^3 (STP)/g, which is 2.98 times greater than the corresponding value for the mHNT-1, 28.313 cm^3 (STP)/g.

The thickness plot patterns of the modified HNTs were similar to those of the unmodified HNTs (Fig. 7b). The inclination increased according to the order of separation, because the samples separated later had larger V_m values and gas-adsorption efficiencies. The gas-adsorption of mHNT-5 at 1.2 nm pore thickness was 191.81 cm^3 (STP)/g, which is 1.52 times greater than that of mHNT-1, which was 125.87 cm^3 (STP)/g.

Transmission electron microscopy images of natural and modified HNTs (Fig. 8, Table 4) were used to determine the average lengths and outer and inner diameters of the HNTs. The TEM images were also utilized to compare the relative differences between the five difference sizes of natural HNTs. The size of the nanotubes tended to decrease with increasing centrifugal force. The nanotube groups were not clearly divided in terms of gas-adsorption capacity because the separation of HNTs was affected by various factors such as mass, hydrophilicity, and the size of each particle.

The largest contribution to separation was assumed to be the mass of the particles. Because the atomic composition of each halloysite is almost the same, as the HNT particle size decreased, the mass of the particle would be decreased

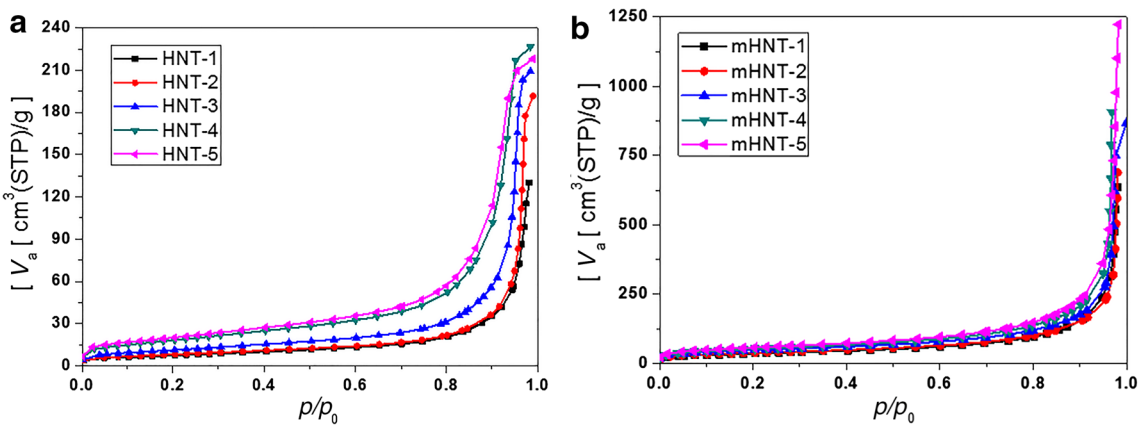

Fig. 5 Adsorption isotherms of five groups of: **a** natural HNT, **b** mHNT (5 M).

https://doi.org/10.1007/s42860-019-00059-4 Published online by Cambridge University Press

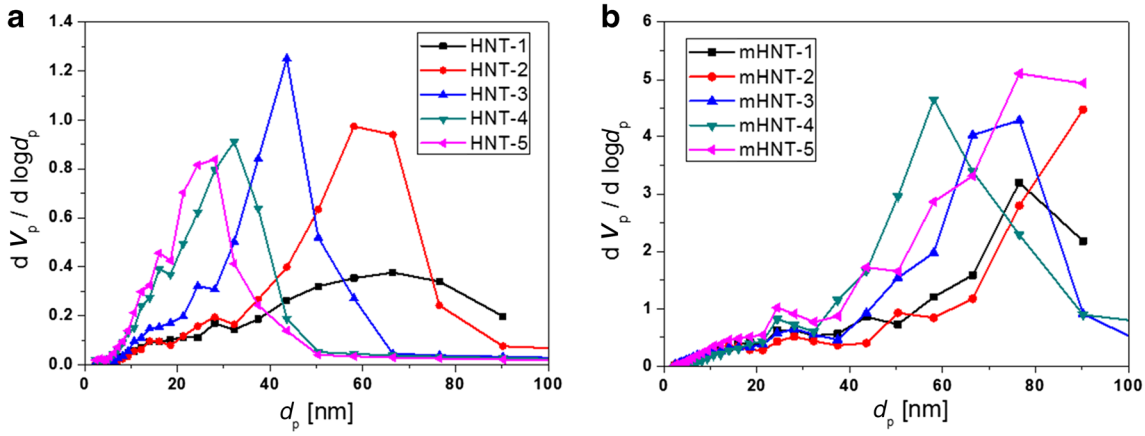

Fig. 6 BJH plots of 5 groups of: **a** natural HNT, **b** mHNT (5 M).

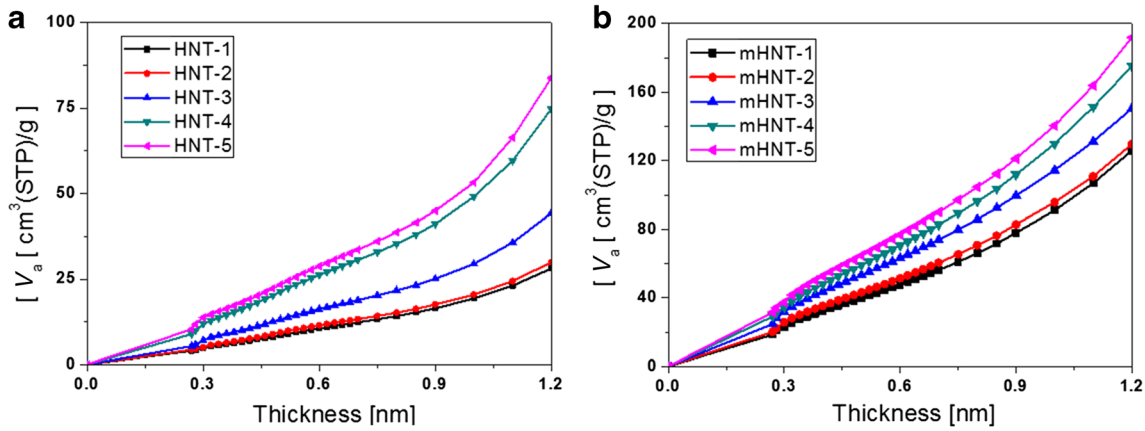

Fig. 7 Thickness plots of five groups of: **a** natural HNT, **b** mHNT (5 M).

proportionally. Therefore, in principle, the gas adsorption capacity of the tubes is inversely proportional to the size of the particles.

HNT-5 had nano-size debris (Fig. 8e). The hindrance of gas-adsorption for this sample was because of these light nanotube fragments that were mixed with the intact tubes.

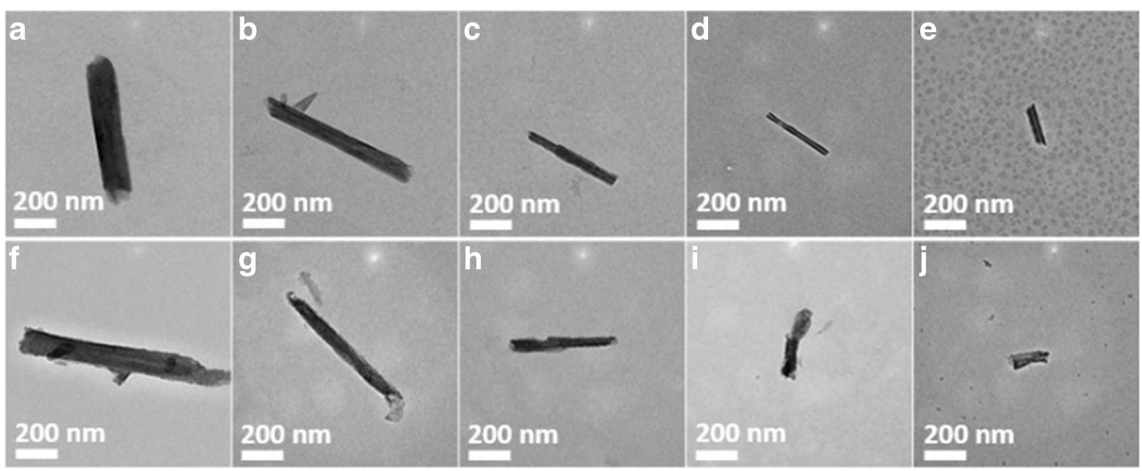

Fig. 8 TEM images of natural HNT groups: **a** HNT-1, **b** HNT-2, **c** HNT-3, **d** HNT-4, **e** HNT-5. TEM images of modified HNT groups: **f** mHNT-1, **g** mHNT-2, **h** mHNT-3, **i** mHNT-4, **j** mHNT-5.

https://doi.org/10.1007/s42860-019-00059-4 Published online by Cambridge University Press

Table 4. Average lengths and outer (O.D.) and inner (I.D.) diameters of the HNTs.

Natural HNT			
	Length (nm)	O.D. (nm)	I.D. (nm)
1	835.36	101.19	33.16
2	699.94	81.44	21.70
3	445.36	76.61	19.47
4	312.14	59.82	14.82
5	212.68	44.99	12.86
Modified HNT (with 5 M sulfuric acid)			
	Length (nm)	O.D. (nm)	I.D. (nm)
1	802.68	103.70	40.85
2	691.98	77.80	27.68
3	450.36	75.13	23.85
4	330.36	66.70	21.25
5	225.72	39.29	14.11

Separated samples of modified HNTs are shown in Fig. 8f–j. They exhibited an increasing gas-adsorption tendency with separation process; the size of the nanotubes decreased according to the order of separation. Therefore, the assumption that the gas-adsorption capacity is inversely proportional to the mass or size of the particles is applied from the same perspective as with separated natural HNTs. The fragments of nanotubes are detectable in the mHNT-5 sample also (Fig. 8j). These experiments demonstrated that the porosity of halloysite nanotubes could be increased by selection of a small size and acid treatment.

SUMMARY

Sulfuric acid was used to increase the porosity of halloysite nanotubes by etching the lumen of the HNT. Modified HNTs were prepared successfully using various concentrations of sulfuric acid. The chemical compositions of modified HNTs were verified by XRD and EDX spectroscopy. This modification selectively removed alumina from the tubes, and decreased the mass of the tubes. Furthermore, the porosity and the inner space of the tubes were clearly increased. The transformation of the tubes increased significantly the gas-adsorption efficiency of the HNTs. The dealumination of the surface increased the inner space, which is very effective for storing other materials within the tubes. The size of the lumen of the modified HNTs was verified by BJH plots and thickness plots. Thus, more materials could be loaded into the HNT tubes. In addition, the separation of smaller HNTs by centrifugation provided an opportunity to maximize the gas-adsorption capacity by excluding low-efficiency groups.

ACKNOWLEDGMENTS

This work was supported by a National Research Foundation of Korea grant (NRF-2019R1F1A1056947).

Compliance with Ethical Statements

Conflict of Interest

The authors declare that they have no conflict of interest.

REFERENCES

Abdullayev, E., Sakakibara, K., Okamoto, K., Wei, W., Ariga, K., & Lvov, Y. (2011). Natural tubule clay template synthesis of silver nanorods for antibacterial composite coating. *ACS Applied Materials & Interfaces, 3*, 4040–4046.

Abdullayev, E., Joshi, A., Wei, W., Zhao, Y., & Lvov, Y. (2012). Enlargement of halloysite clay nanotube lumen by selective etching of aluminum oxide. *ACS Nano, **6***, 7216–7226.

Baiju, K., Shukla, S., Biju, S., Reddy, M., & Warrier, K. (2009). Hydrothermal processing of dye-adsorbing one-dimensional hydrogen titanate. *Materials Letters, **63***, 923–926.

Barrett, E. P., Joyner, L. G., & Halenda, P. P. (1951). The determination of pore volume and area distributions in porous substances. I. Computations from nitrogen isotherms. *Journal of the American Chemical Society, **73***, 373–380.

Chao, C., Liu, J., Wang, J., Zhang, Y., Zhang, B., Zhang, Y., Xiang, X., & Chen, R. (2013). Surface modification of halloysite nanotubes with dopamine for enzyme immobilization. *ACS Applied Materials & Interfaces, **5***, 10559–10564.

Costanzo, P., & Giese, R. (1985). Dehydration of synthetic hydrated kaolinites: a model for the dehydration of halloysite (10 Å). *Clays and Clay Minerals, 33*, 415–423.

De Silva, R., Pasbakhsh, P., Goh, K., Chai, S.-P., & Ismail, H. (2013). Physico-chemical characterisation of chitosan/halloysite composite membranes. *Polymer Testing, 32*, 265–271.

Gorrasi, G. (2015). Dispersion of halloysite loaded with natural antimicrobials into pectins: characterization and controlled release analysis. *Carbohydrate Polymers, 127*, 47–53.

Guimaraes, L., Enyashin, A. N., Seifert, G., & Duarte, H. A. (2010). Structural, electronic, mechanical properties of single-walled halloysite nanotube models. *Journal of Physical Chemistry C, 114*, 11358–11363.

Guo, M., Wang, A., Muhammad, F., Qi, W., Ren, H., Guo, Y., & Zhu, G. (2012). Halloysite nanotubes, a multifunctional nanovehicle for anticancer drug delivery. *Chinese Journal of Chemistry, 30*, 2115–2120.

Hong, C. H., Liu, Y. D., & Choi, H. J. (2013). Carbonyl iron suspension with halloysite additive and its magnetorheology. *Applied Clay Science, 80*, 366–371.

Joo, Y., Sim, J. H., Jeon, Y., Lee, S. U., & Sohn, D. (2013). Opening and blocking the inner-pores of halloysite. *Chemical Communications, 49*, 4519–4521.

Kamble, R., Ghag, M., Gaikawad, S., & Panda, B. K. (2012). Halloysite nanotubes and applications: a review. *Journal of Advanced Scientific Research, 3*, 25–29.

Kaneko, K. (1994). Determination of pore size and pore size distribution: 1. Adsorbents and catalysts. *Journal of Membrane Science, 96*, 59–89.

Ko, J., Lee, J., Yoo, B., Ryu, J., & Sohn, D. (2016). Capillarity-induced selective ex-situ synthesis of metal–organic framework inside mesoporous nanotubes. *Microporous and Mesoporous Materials, 220*, 16–20.

Lazzara, G., Cavallaro, G., Panchal, A., Fakhrullin, R., Stavitskaya, A., Vinokurov, V., & Lvov, Y. (2018). An assembly of organic-inorganic composites using halloysite clay nanotubes. *Current Opinion in Colloid & Interface Science, 35*, 42–50.

Lippens, B. C., & De Boer, J. (1965). Studies on pore systems in catalysts: V. The t method. *Journal of Catalysis, 4*, 319–323.

Liu, M., Zhang, Y., Wu, C., Xiong, S., & Zhou, C. (2012). Chitosan/halloysite nanotubes bionanocomposites: structure, mechanical

https://doi.org/10.1007/s42860-019-00059-4 Published online by Cambridge University Press

properties and biocompatibility. *International Journal of Biological Macromolecules, 51*, 566–575.

Luan, Z., He, H., Zhou, W., Cheng, C.-F., & Klinowski, J. (1995). Effect of structural aluminium on the mesoporous structure of MCM-41. *Journal of the Chemical Society, Faraday Transactions, 91*, 2955–2959.

Luo, Z., Song, H., Feng, X., Run, M., Cui, H., Wu, L., Gao, J., & Wang, Z. (2013). Liquid crystalline phase behavior and sol–gel transition in aqueous halloysite nanotube dispersions. *Langmuir, 29*, 12358–12366.

Lvov, Y., Aerov, A., & Fakhrullin, R. (2014). Clay nanotube encapsulation for functional biocomposites. *Advances in Colloid and Interface Science, 207*, 189–198.

Lvov, Y., Wang, W., Zhang, L., & Fakhrullin, R. (2016). Halloysite clay nanotubes for loading and sustained release of functional compounds. *Advanced Materials, 28*, 1227–1250.

Massaro, M., Riela, S., Cavallaro, G., Gruttadauria, M., Milioto, S., Noto, R., & Lazzara, G. (2014). Eco-friendly functionalization of natural halloysite clay nanotube with ionic liquids by microwave irradiation for Suzuki coupling reaction. *Journal of Organometallic Chemistry, 749*, 410–415.

Mroczek, K., Kalisz, S., Pronobis, M., & Sołtys, J. (2011). The effect of halloysite additive on operation of boilers firing agricultural biomass. *Fuel Processing Technology, 92*, 845–855.

Owoseni, O., Nyankson, E., Zhang, Y., Adams, S. J., He, J., McPherson, G. L., Bose, A., Gupta, R. B., & John, V. T. (2014). Release of surfactant cargo from interfacially-active halloysite clay nanotubes for oil spill remediation. *Langmuir, 30*, 13533–13541.

Schull, C. (1948). The determination of pore size distribution from gas adsorption data. *Journal of the American Chemical Society, 70*, 1405–1410.

Shi, Y.-F., Tian, Z., Zhang, Y., Shen, H.-B., & Jia, N.-Q. (2011). Functionalized halloysite nanotube-based carrier for intracellular delivery of antisense oligonucleotides. *Nanoscale Research Letters, 6*, 608.

Shu, Z., Chen, Y., Zhou, J., Li, T., Yu, D., & Wang, Y. (2015). Nanoporous-walled silica and alumina nanotubes derived from halloysite: controllable preparation and their dye adsorption applications. *Applied Clay Science, 112*, 17–24.

Szczepanik, B., Słomkiewicz, P., Garnuszek, M., Rogala, P., Banaś, D., Kubala-Kukuś, A., & Stabrawa, I. (2017). Effect of temperature on halloysite acid treatment for efficient chloroaniline removal from aqueous solutions. *Clays and Clay Minerals, 65*, 155–167.

Tan, D., Yuan, P., Annabi-Bergaya, F., Yu, H., Liu, D., Liu, H., & He, H. (2013). Natural halloysite nanotubes as mesoporous carriers for the loading of ibuprofen. *Microporous and Mesoporous Materials, 179*, 89–98.

Tazaki, K. (2005). Microbial formation of a halloysite-like mineral. *Clays and Clay Minerals, 53*, 224–233.

Vergaro, V., Abdullayev, E., Lvov, Y. M., Zeitoun, A., Cingolani, R., Rinaldi, R., & Leporatti, S. (2010). Cytocompatibility and uptake of halloysite clay nanotubes. *Biomacromolecules, 11*, 820–826.

Wu, H., Watanabe, H., Ma, W., Fujimoto, A., Higuchi, T., Uesugi, K., Takeuchi, A., Suzuki, Y., Jinnai, H., & Takahara, A. (2013). Robust liquid marbles stabilized with surface-modified halloysite nanotubes. *Langmuir, 29*, 14971–14975.

Wu, X., Liu, C., Qi, H., Zhang, X., Dai, J., Zhang, Q., Zhang, L., Wu, Y., & Peng, X. (2016). Synthesis and adsorption properties of halloysite/carbon nanocomposites and halloysite-derived carbon nanotubes. *Applied Clay Science, 119*, 284–293.

Xi, L., Xiaojie, J., Rui, X., Jiang, M., Jie, W., & Liangyin, C. (2013). Halloysite nanotube composited thermo-responsive hydrogel system for controlled-release. *Chinese Journal of Chemical Engineering, 21*, 991–998.

Yah, W. O., Takahara, A., & Lvov, Y. M. (2012a). Selective modification of halloysite lumen with octadecylphosphonic acid: new inorganic tubular micelle. *Journal of the American Chemical Society, 134*, 1853–1859.

Yah, W. O., Xu, H., Soejima, H., Ma, W., Lvov, Y., & Takahara, A. (2012b). Biomimetic dopamine derivative for selective polymer modification of halloysite nanotube lumen. *Journal of the American Chemical Society, 134*, 12134–12137.

Zhang, A.-B., Pan, L., Zhang, H.-Y., Liu, S.-T., Ye, Y., Xia, M.-S., & Chen, X.-G. (2012). Effects of acid treatment on the physicochemical and pore characteristics of halloysite. *Colloids and Surfaces A: Physicochemical and Engineering Aspects, 396*, 182–188.

(*Received 5 September 2019; revised 18 December 2019; AE: Jun Kawamata*)